Supporting Information: Computationally accelerated discovery of high entropy pyrochlore oxides

Krishna Chaitanya Pitike,[1] Antonio Macias,[2] Markus Eisenbach,[3] Craig A. Bridges,[4] and Valentino R. Cooper[1,*]

[1]*Materials Science and Technology Division, Oak Ridge National Laboratory, Oak Ridge, Tennessee 37831, USA*

[2]*Department of Chemistry, University of California, Berkeley, CA 94720, USA*

[3]*National Center for Computational Sciences, Oak Ridge National Laboratory, Oak Ridge, Tennessee 37831, USA*

[4]*Chemical Sciences Division, Oak Ridge National Laboratory, Oak Ridge, Tennessee 37831, USA*

(Dated: April 9, 2021)

* coopervr@ornl.gov

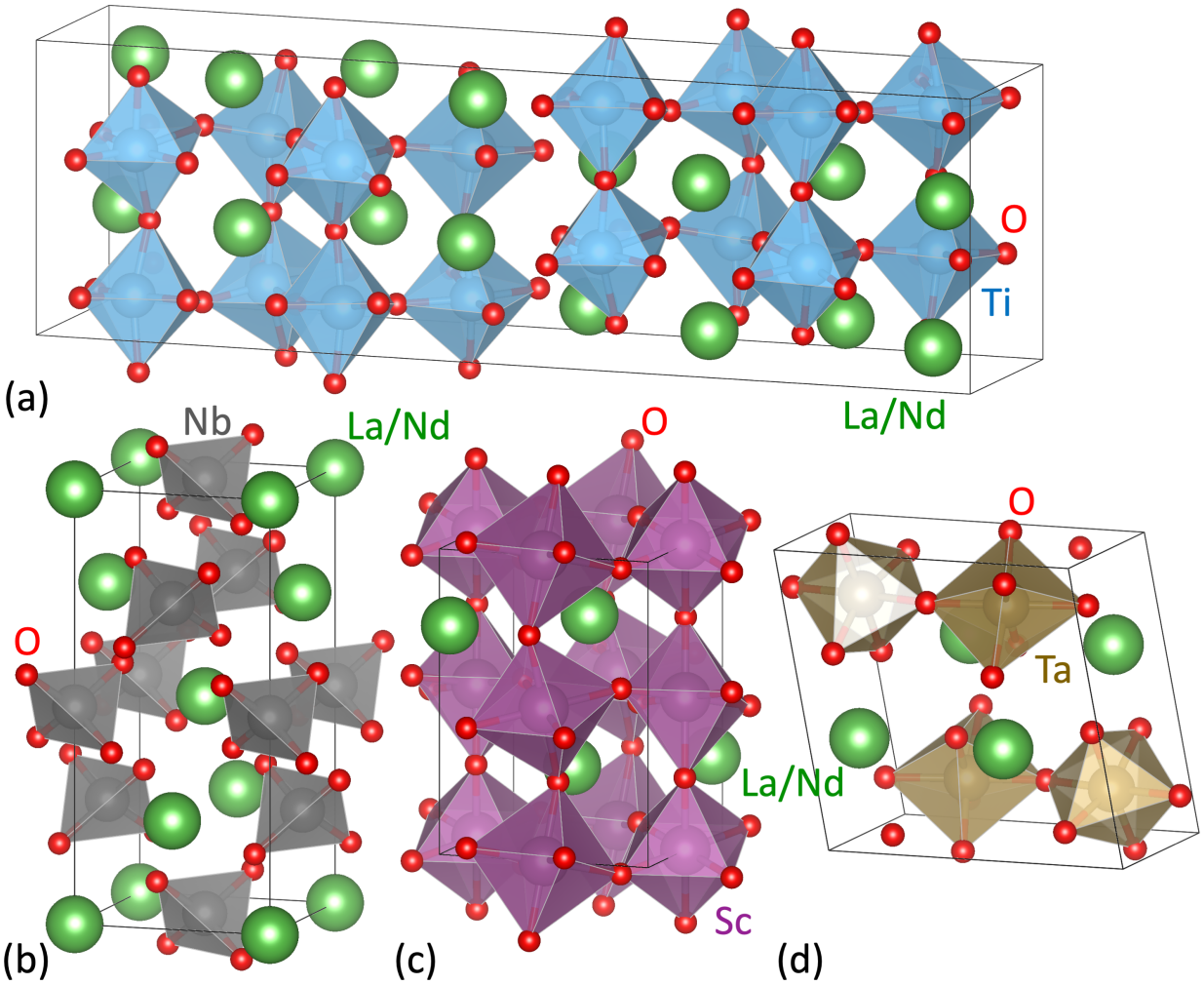

FIG. 1. Structural models used for estimating mixing enthalpies in (a) Perovskite Related Layered Orthorhombic (PRLO), (b) Fergusonite, (c) Perovskite, (d) LaTaO4 structures.

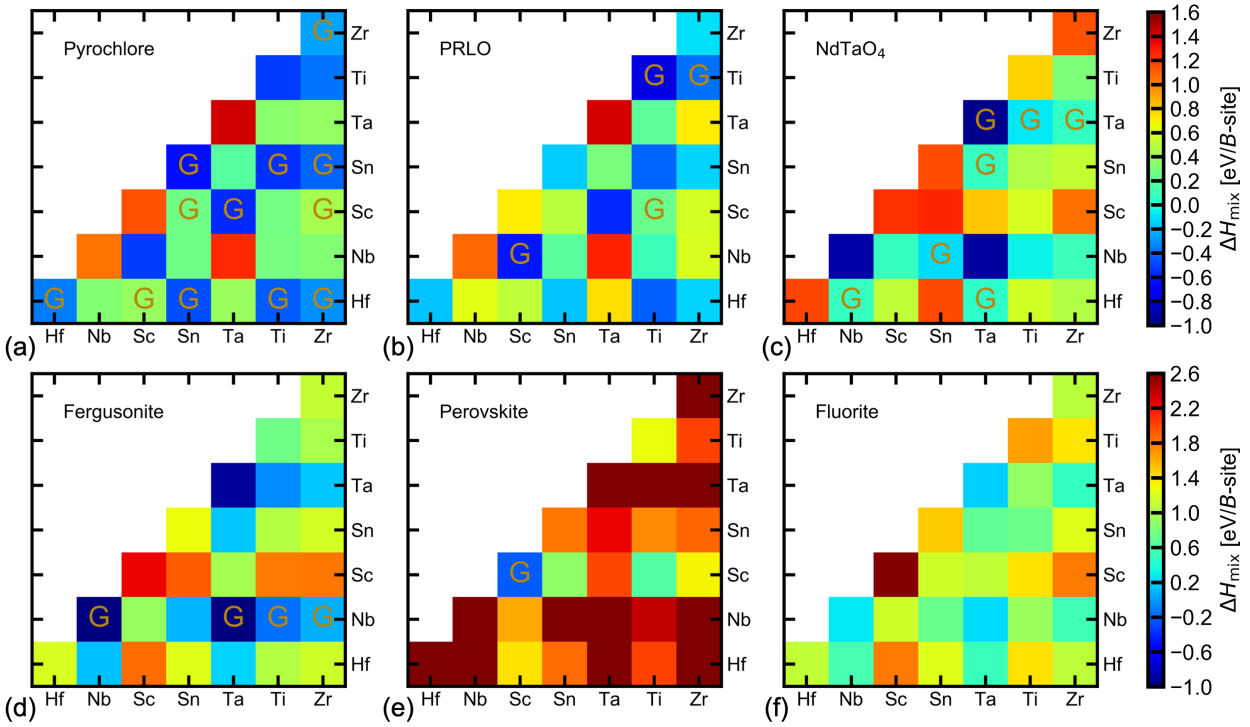

FIG. 2. Heat maps for mixing enthalpy in eV/$B-$site of $Nd_2(BB^{'})_2O_n$ two component ternary oxides in phase P, $\Delta H_{\rm mix}[A_2(BB^{'})_2O_n, P]$, calculated from first principles using Eq. 1 of main text. Presented for (**a**) pyrochlore, (**b**) PRLO, (**c**) $NdTaO_4$, (**d**) fluorite, (**e**) fergusonite and (**f**) perovskite phases. The annotation 'G' in each panel represents the *ground phase* for the two cation combination.

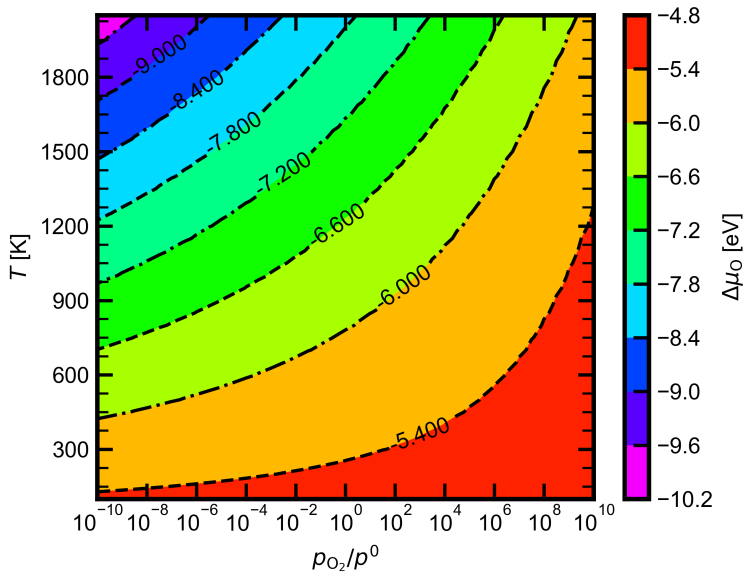

FIG. 3. Contour heat map plotted for $\Delta\mu_{\mathrm{O}}$ as a function of T and p_{O_2}/p^0. The mathematical formula for the evaluation of $\Delta\mu_{\mathrm{O}}$ is given in Eq. 2 of main text. The horizontal axis is plotted on log scale.

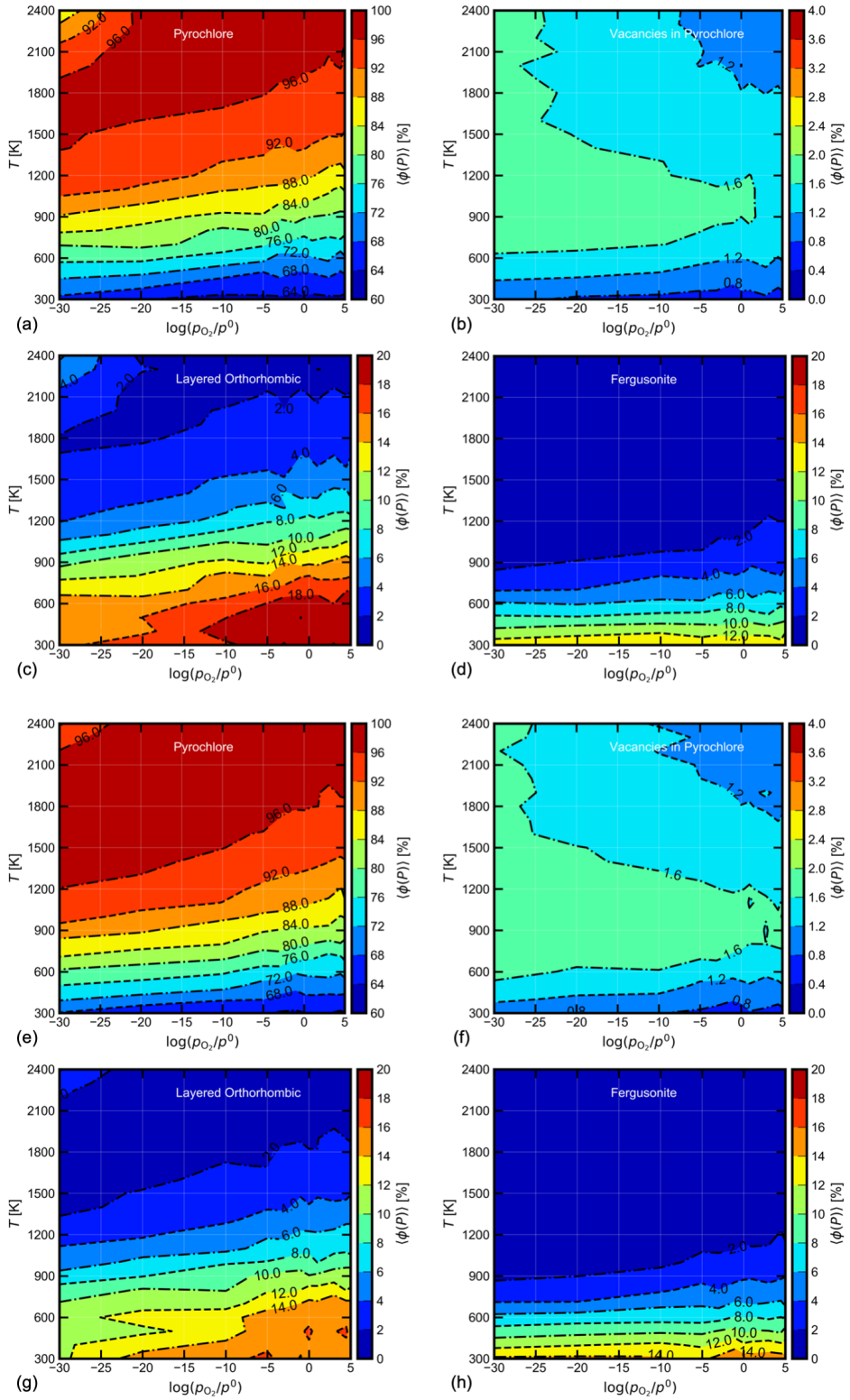

FIG. 4. Heat map of $\langle\phi(P)\rangle$ plotted as a function of T and p_{O_2}/p^0 for $A_2B_2O_7$. **(a-d)** A = La and B = {Hf,Nb,Sc,Sn,Zr} and **(e-h)** A = Nd and B = {Hf,Nb,Sc,Sn,Zr}. The contour lines along with their annotated values are also given for each panel.

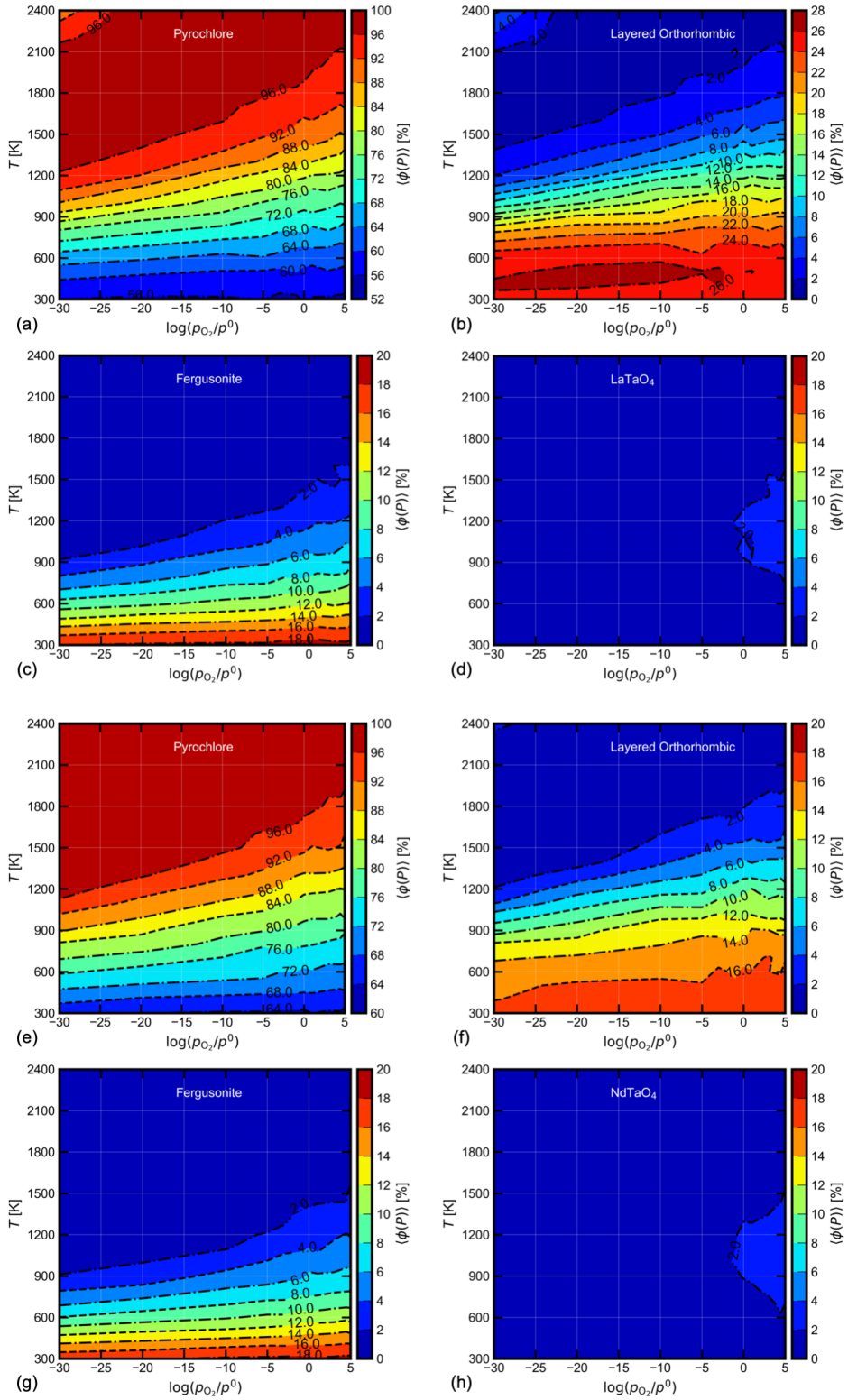

FIG. 5. Heat map of $\langle\phi(P)\rangle$ plotted as a function of T and p_{O_2}/p^0 for $A_2B_2O_7$. **(a-d)** A = La and $B = \{$Hf,Nb,Sn,Ti,Zr$\}$ and **(e-h)** A = Nd and $B = \{$Hf,Nb,Sn,Ti,Zr$\}$. The contour lines along with their annotated values are also given for each panel.

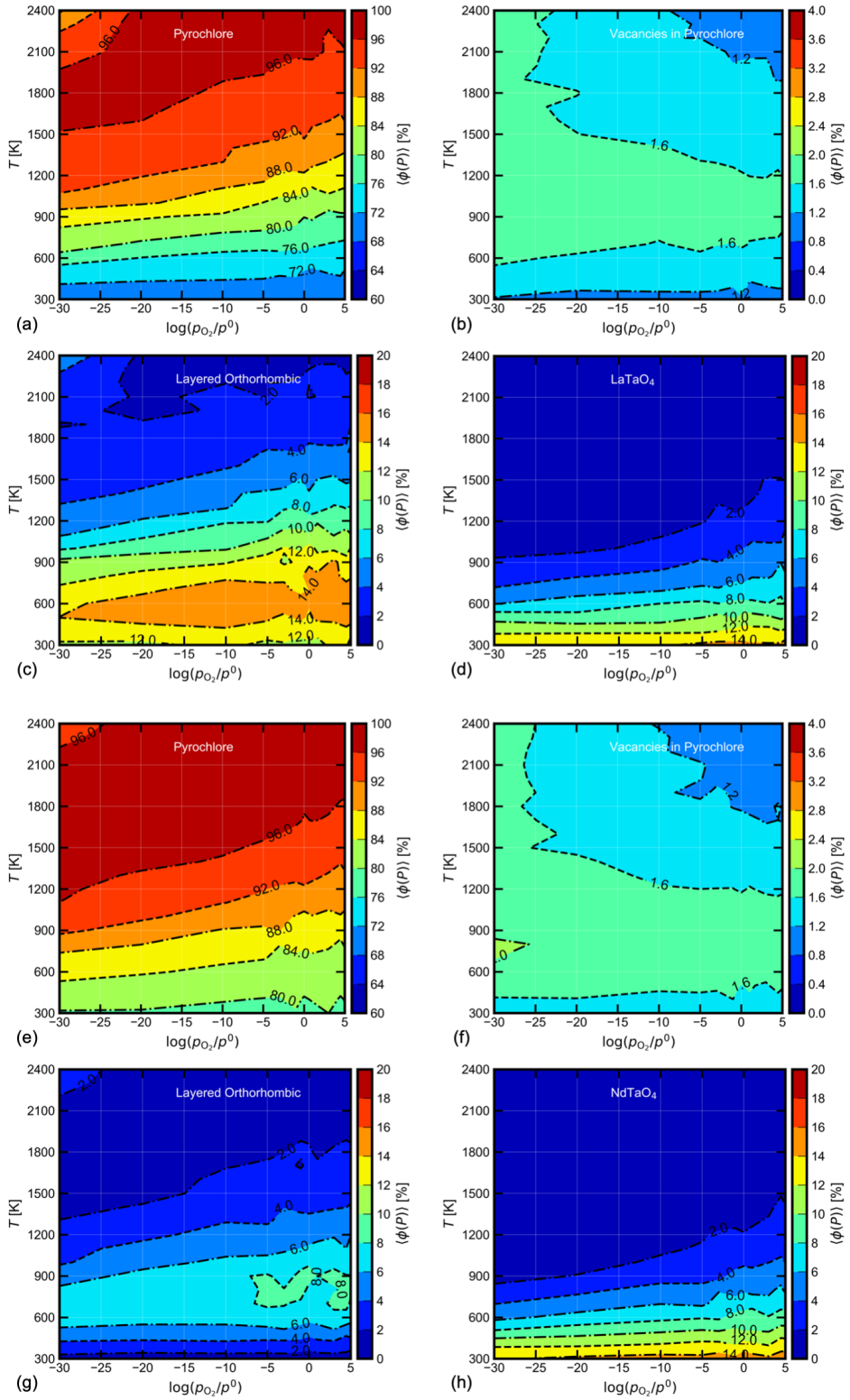

FIG. 6. Heat map of $\langle\phi(P)\rangle$ plotted as a function of T and p_{O_2}/p^0 for $A_2B_2O_7$. **(a-d)** $A =$ La and $B =$ {Hf,Sc,Sn,Ta,Zr} and **(e-h)** $A =$ Nd and $B =$ {Hf,Sc,Sn,Ta,Zr}. The contour lines along with their annotated values are also given for each panel.

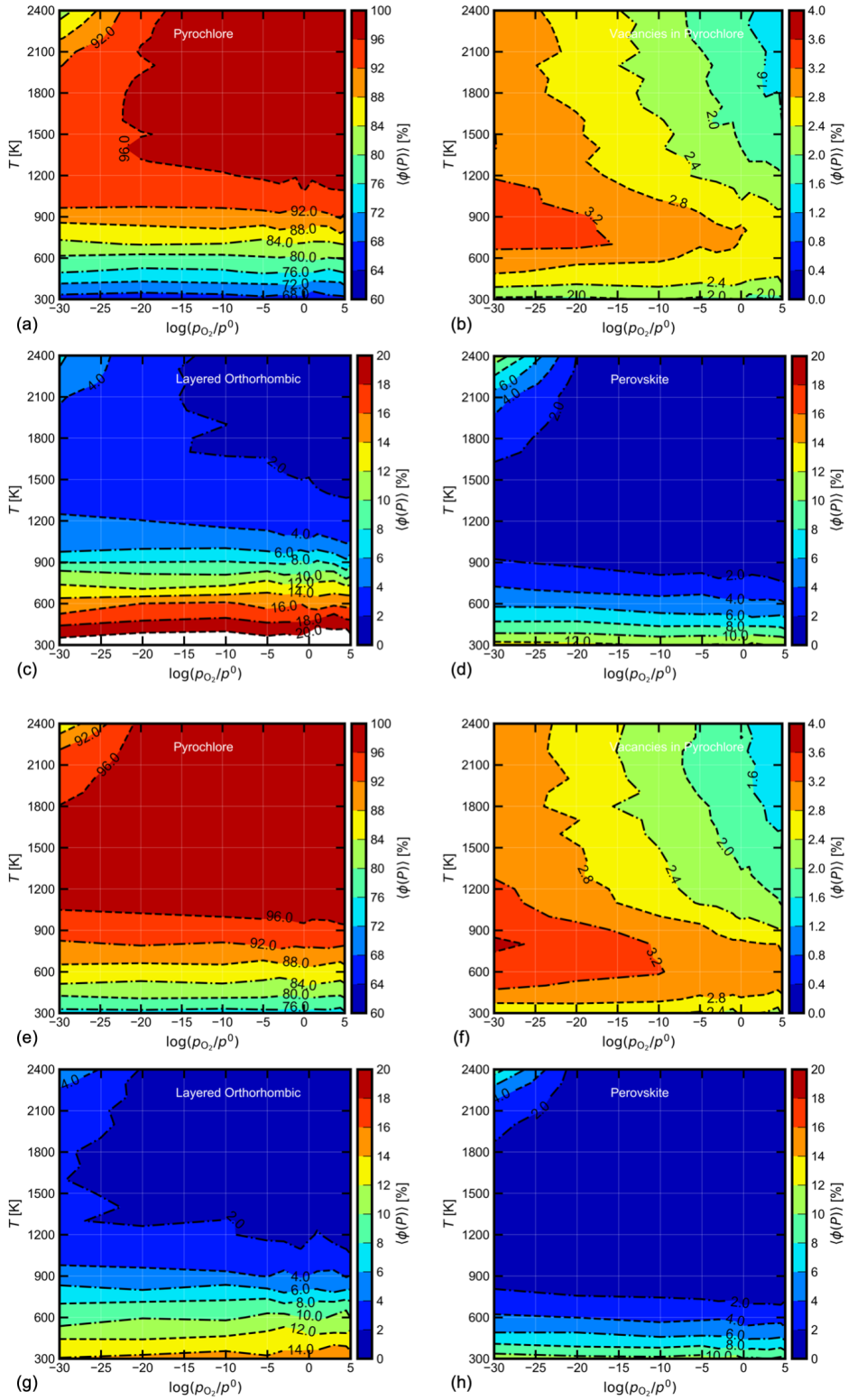

FIG. 7. Heat map of $\langle\phi(P)\rangle$ plotted as a function of T and p_{O_2}/p^0 for $A_2B_2O_7$. **(a-d)** $A =$ La and $B =$ {Hf,Sc,Sn,Ti,Zr} and **(e-h)** $A =$ Nd and $B =$ {Hf,Sc,Sn,Ti,Zr}. The contour lines along with their annotated values are also given for each panel.

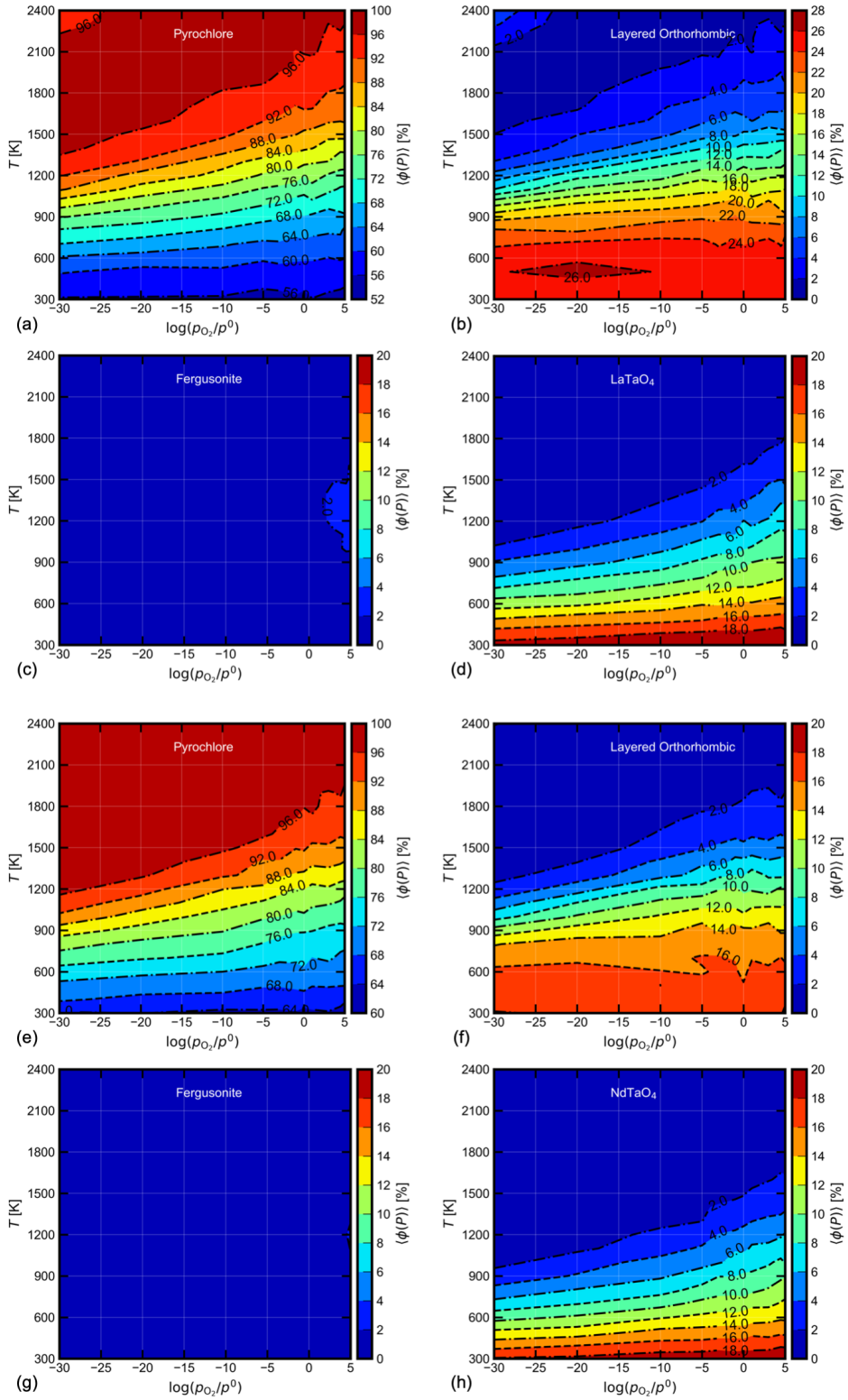

FIG. 8. Heat map of $\langle\phi(P)\rangle$ plotted as a function of T and p_{O_2}/p^0 for $A_2B_2O_7$. **(a-d)** $A =$ La and $B =$ {Hf,Sn,Ta,Ti,Zr} and **(e-h)** $A =$ Nd and $B =$ {Hf,Sn,Ta,Ti,Zr}. The contour lines along with their annotated values are also given for each panel.

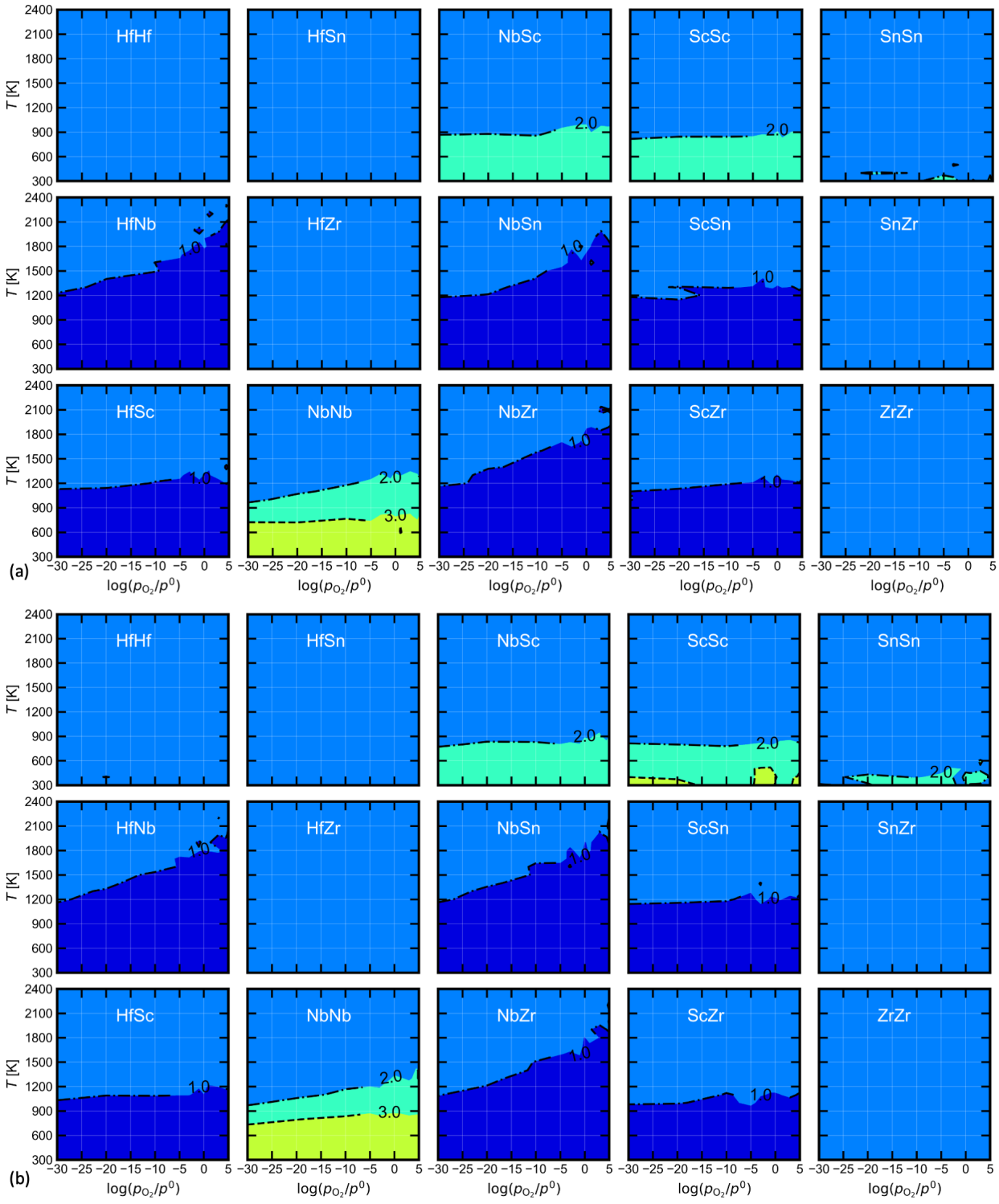

FIG. 9. Heat map of short range order parameter for each two component combination for $A_2B_2O_7$ is plotted in separate panel as a function of $\log(p_{O_2}/p^0)$ and T. **(a)** $A =$ La and $B = \{$Hf,Nb,Sc,Sn,Zr$\}$ and **(b)** $A =$ Nd and $B = \{$Hf,Nb,Sc,Sn,Zr$\}$. The contour lines along with their annotated values are also given for each panel.

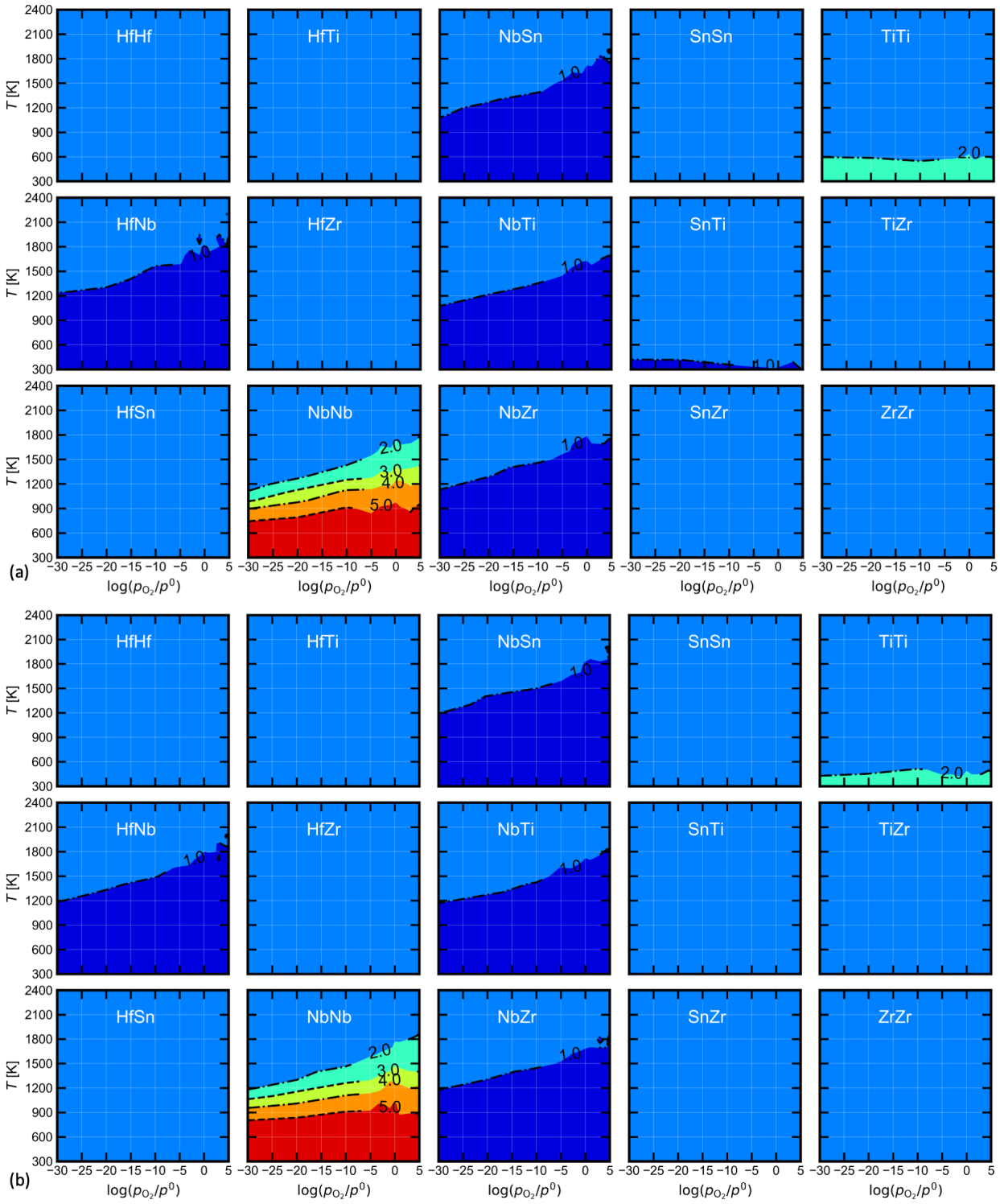

FIG. 10. Heat map of short range order parameter for each two component combination for $A_2B_2O_7$ is plotted in separate panel as a function of $\log(p_{O_2}/p^0)$ and T. **(a)** $A =$ La and $B = \{$Hf,Nb,Ti,Sn,Zr$\}$ and **(b)** $A =$ Nd and $B = \{$Hf,Nb,Ti,Sn,Zr$\}$. The contour lines along with their annotated values are also given for each panel.

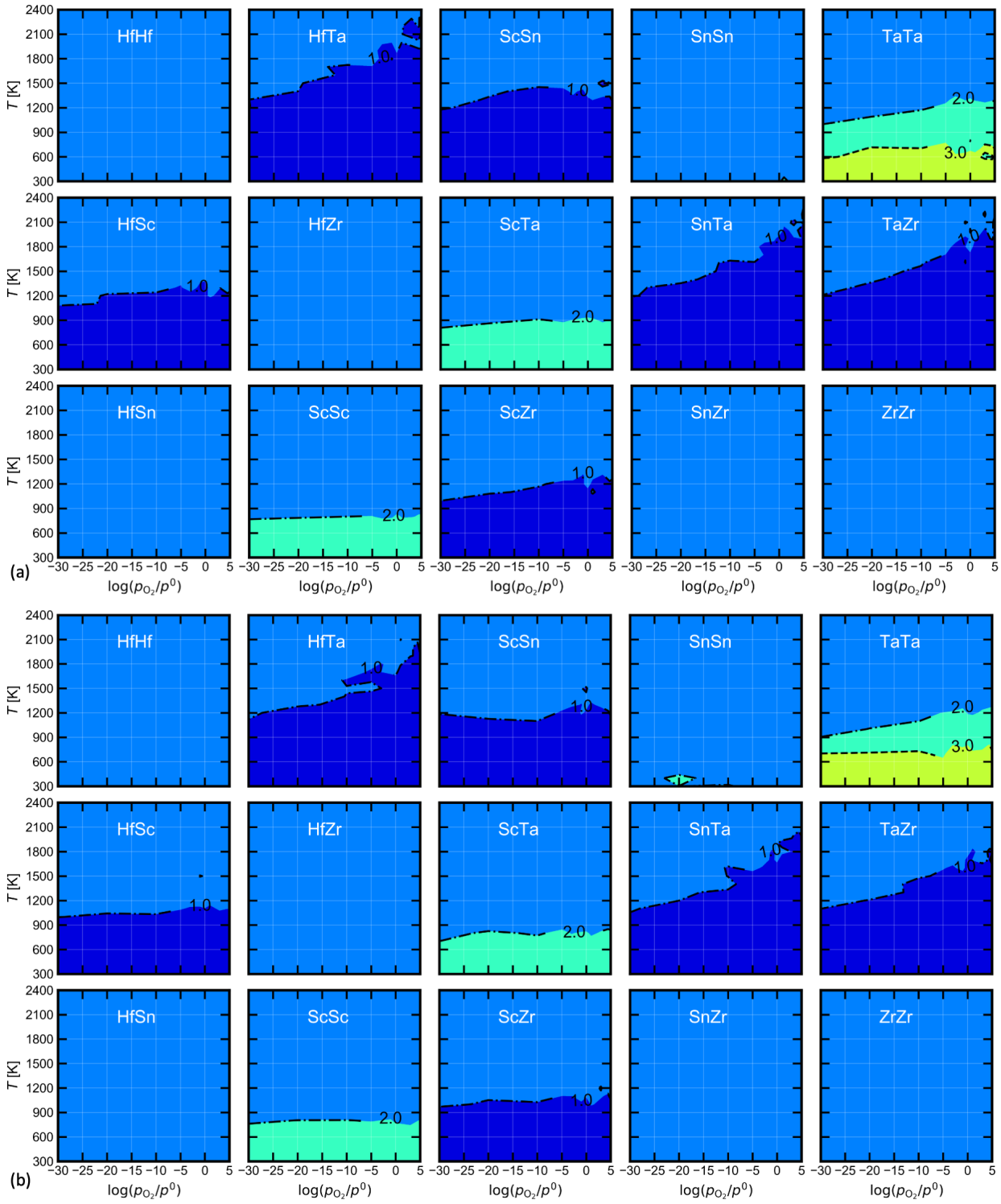

FIG. 11. Heat map of short range order parameter for each two component combination for $A_2B_2O_7$ is plotted in separate panel as a function of $\log(p_{O_2}/p^0)$ and T. **(a)** $A =$ La and $B = \{$Hf,Sc,Sn,Ta,Zr$\}$ and **(b)** $A =$ Nd and $B = \{$Hf,Sc,Sn,Ta,Zr$\}$. The contour lines along with their annotated values are also given for each panel.

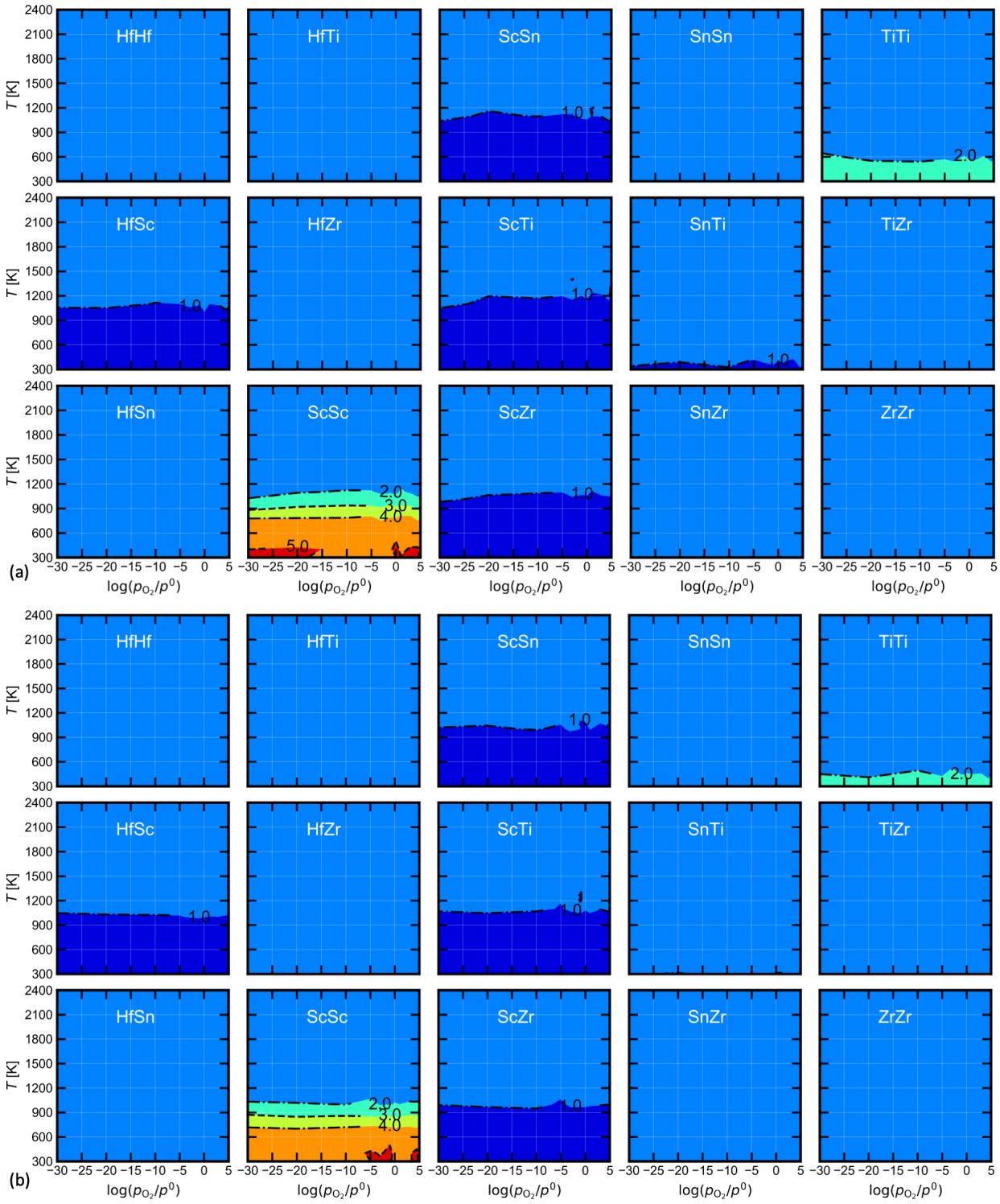

FIG. 12. Heat map of short range order parameter for each two component combination for $A_2B_2O_7$ is plotted in separate panel as a function of $\log(p_{O_2}/p^0)$ and T. **(a)** $A =$ La and $B = \{$Hf,Sc,Sn,Ti,Zr$\}$ and **(b)** $A =$ Nd and $B = \{$Hf,Sc,Sn,Ti,Zr$\}$. The contour lines along with their annotated values are also given for each panel.

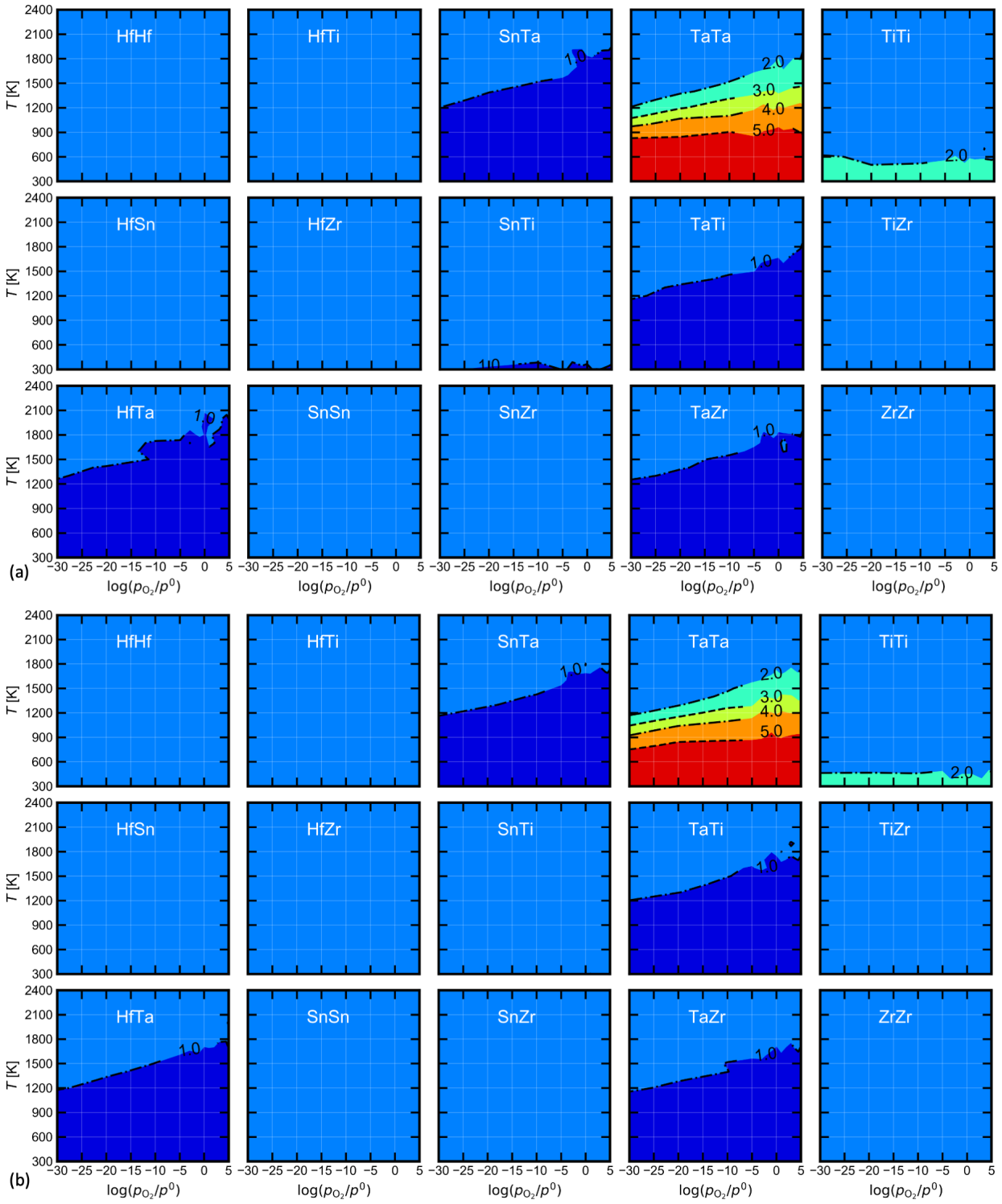

FIG. 13. Heat map of short range order parameter for each two component combination for $A_2B_2O_7$ is plotted in separate panel as a function of $\log(p_{O_2}/p^0)$ and T. **(a)** $A =$ La and $B = \{$Hf,Sn,Ta,Ti,Zr$\}$ and **(b)** $A =$ Nd and $B = \{$Hf,Sn,Ta,Ti,Zr$\}$. The contour lines along with their annotated values are also given for each panel.

TABLE I. The ground state structures of the ternary compounds along with their space group symmetries. The fergusonite and scheelite structures are equivalent, whereas the $YNbO_4$ structure is obtained through a monoclinic distortion of the fergusonite structure. Hence, to avoid confusion we refer to all these structures as fergusonite. Also, even though there are multiple polymorphs [1] for $NdTaO_4$, the structures and their energies are very close.

Index	A	B	Compound	Ground state strucurue	Symmetry	Ref.
1	La	Hf	$La_2Hf_2O_7$	Pyrochlore	$Fd\bar{3}m$	[2]
2	La	Nb	$La_2Nb_2O_8$	Fergusonite	$I4_1/a$	[3]
3	La	Sc	$La_2Sc_2O_6$	Perovskite	$Pbnm$	[4]
4	La	Sn	$La_2Sn_2O_7$	Pyrochlore	$Fd\bar{3}m$	[5, 6]
5	La	Ta	$La_2Ta_2O_8$	$LaTaO_4$	P_12_1/c_1	[7]
6	La	Ti	$La_2Ti_2O_7$	PRLO	$Pna2_1$	[8]
7	La	Zr	$Nd_2Zr_2O_7$	Pyrochlore	$Fd\bar{3}m$	[2, 9]
8	Nd	Hf	$Nd_2Hf_2O_7$	Pyrochlore	$Fd\bar{3}m$	[10]
9	Nd	Nb	$Nd_2Nb_2O_8$	$YNbO_4$	I_12/c_1	[11]
10	Nd	Sc	$Nd_2Sc_2O_6$	Perovskite	$Pbnm$	[4]
11	Nd	Sn	$Nd_2Sn_2O_7$	Pyrochlore	$Fd\bar{3}m$	[6]
12	Nd	Ta	$Nd_2Ta_2O_8$	$NdTaO_4$	P_12_1/c_1	[12]
13	Nd	Ti	$Nd_2Ti_2O_7$	PRLO	$Pna2_1$	[13]
14	Nd	Zr	$Nd_2Zr_2O_7$	Pyrochlore	$Fd\bar{3}m$	[14]

TABLE II. Pseudo potential files and electronic configuration used in this study. For Nd we used only one valance electron in the $4f$ valance states, and the remaining three electrons are included in the core potential.

	Elemental species	VASP PAW potential	Valance electrons	Electronic configuration
1	La	La	11	$5s^2 5p^6 6s^2 5d^1$
2	Nd	Nd_3	11	$5s^2 5p^6 6s^2 4f^1$
3	Hf	Hf_sv	12	$5s^2 5p^6 6s^2 5d^2$
4	Nb	Nb_sv	13	$4s^2 4p^6 5s^1 4d^4$
5	Sc	Sc_sv	11	$3s^2 3p^6 4s^2 3d^1$
6	Sn	Sn_d	14	$5s^2 4d^{10} 5p^2$
7	Ta	Ta_pv	11	$5s^2 5p^6 6s^2 5d^3$
8	Ti	Ti_sv	12	$3p^6 4s^2 3d^4$
9	Zr	Zr_sv	12	$4s^2 4p^6 5s^2 4d^2$
10	O	O	6	$2s^2 p^4$

TABLE III. Symmetry, Wyckoff symbols and coordinates of pyrochlore and fluorite structures.

Sl.No.	Structure	Space group	Wyckoff symbol	Element	Coordinates
1	Pyrochlore	F$d\bar{3}m$	16 c	A	(0.000, 0.000, 0.000)
2			16 d	B	(0.500, 0.500, 0.500)
3			8 a	O1	(0.375, 0.375, 0.375)
4			48 f	O2	(0.329, 0.125, 0.125)
1	Fluorite	F$d\bar{3}m$	16 c	A	(0.000, 0.000, 0.000)
2			16 d	B	(0.500, 0.500, 0.500)
3			16 a	O1	(0.125, 0.125, 0.125)
4			16 b	O2	(0.375, 0.125, 0.125)
5			16 f	O3	(0.625, 0.125, 0.125)

[1] M. Nyman, M. A. Rodriguez, L. E. Rohwer, J. E. Martin, M. Waller, and F. E. Osterloh, Unique $LaTaO_4$ polymorph for multiple energy applications, Chem. Mater. **21**, 4731 (2009).

[2] K. R. Whittle, L. M. Cranswick, S. A. Redfern, I. P. Swainson, and G. R. Lumpkin, Lanthanum pyrochlores and the effect of yttrium addition in the systems $La_{2-x}Y_xZr_2O_7$ and $La_{2-x}Y_xHf_2O_7$, J. Sol. State Chem. **182**, 442 (2009).

[3] P. Sarin, R. W. Hughes, D. R. Lowry, Z. D. Apostolov, and W. M. Kriven, High-temperature properties and ferroelastic phase transitions in rare-earth niobates ($LnNbO_4$), J. Am. Ceram. Soc. **97**, 3307 (2014).

[4] R. P. Liferovich and R. H. Mitchell, A structural study of ternary lanthanide orthoscandate perovskites, J. Sol. State Chem. **177**, 2188 (2004).

[5] V. Bondah-Jagalu and S. T. Bramwell, Magnetic susceptibility study of the heavy rare-earth stannate pyrochlores, Can. J. Phys. **79**, 1381 (2001).

[6] B. J. Kennedy, Structural trends in pyrochlore oxides, Mater. Sci. Forum **228**, 753 (1996).

[7] T. Kurova and V. Aleksandrov, Crystalline structure of $LaTaO_4$, Doklady Akademii Nauk SSSR **201**, 1095 (1971).

[8] M. Gasperin, Dititanate de lanthane, Acta Crystallogr. B Struct. Cryst. Cryst. Chem. **31**, 2129 (1975).

[9] Y. Tabira, R. L. Withers, L. Minervini, and R. W. Grimes, Systematic structural change in selected rare earth oxide pyrochlores as determined by wide-angle CBED and a comparison with the results of atomistic computer simulation, J. Sol. State Chem. **153**, 16 (2000).

[10] V. K. Anand, A. K. Bera, J. Xu, T. Herrmannsdörfer, C. Ritter, and B. Lake, Observation of long-range magnetic ordering in pyrohafnate $Nd_2Hf_2O_7$: A neutron diffraction study, Phys. Rev. B **92** (2015).

[11] S. Tsunekawa, T. Kamiyama, K. Sasaki, H. Asano, and T. Fukuda, Precise structure analysis by neutron diffraction for $RNbO_4$ and distortion of NbO_4 tetrahedra, Acta Crystallogr. A **49**, 595 (1993).

[12] Y. Titov, A. Sych, A. Sokolov, A. Kapshuk, V. Markiv, and N. Belyavina, Crystal structure of the high-pressure modification of $NdTaO_4$, J. Alloys Compd. **311**, 252 (2000).

[13] N. Ishizawa, K. Ninomiya, T. Sakakura, and J. Wang, Redetermination of $Nd_2Ti_2O_7$: a non-centrosymmetric structure with perovskite-type slabs, Acta Crystallogr. E **69**, i19 (2013).

[14] M. van Dijk, J. ter Maat, G. Roelofs, H. Bosch, G. van de Velde, P. Gellings, and A. Burggraaf, Electrical and catalytic properties of some oxides with the fluorite or pyrochlore structure, Mater. Res. Bull. **19**, 1149 (1984).